

Mukund Narasimhan
Department of Electrical & Computer
Engineering,
University of Nevada,
Las Vegas, NV 89154-4026

Haibo Dong
e-mail: haibo@gwu.edu

Rajat Mittal
e-mail: mittal@gwu.edu

Department of Mechanical and Aerospace
Engineering,
The George Washington University,
Washington DC 22052

Sahjendra N. Singh
Department of Electrical & Computer
Engineering,
University of Nevada,
Las Vegas, NV 89154-4026
e-mail: sahaj@ee.unlv.edu

Optimal Yaw Regulation and Trajectory Control of Biorobotic AUV Using Mechanical Fins Based on CFD Parametrization¹

This paper treats the question of control of a biorobotic autonomous undersea vehicle (BAUV) in the yaw plane using a biomimetic mechanism resembling the pectoral fins of fish. These fins are assumed to undergo a combined sway-yaw motion and the bias angle is treated as a control input, which is varied in time to accomplish the maneuver in the yaw-plane. The forces and moments produced by the flapping foil are parametrized using computational fluid dynamics. A finite-difference-based, Cartesian grid immersed boundary solver is used to simulate flow past the flapping foils. The periodic forces and moments are expanded as a Fourier series and a discrete-time model of the BAUV is developed for the purpose of control. An optimal control system for the set point control of the yaw angle and an inverse control law for the tracking of time-varying yaw angle trajectories are designed. Simulation results show that in the closed-loop system, the yaw angle follows commanded sinusoidal trajectories and the segments of the intersample yaw trajectory remain close to the discrete-time reference trajectory. It is also found that the fins suitably located near the center of mass of the vehicle provide better maneuverability. [DOI: 10.1115/1.2201634]

Keywords: biorobotic AUV, yaw-plane control, CFD, pectoral fins

1 Introduction

Aquatic animals present a wide diversity of maneuvering behaviors and hydrodynamic mechanisms for their locomotion. Fish use a variety of fins (dorsal, caudal, pectoral, pelvic fins, etc.) for maneuvering and propulsion [1,2]. Biological studies is motivating researchers to design biorobotic autonomous underwater vehicles (BAUVs) actuated by oscillating fins for naval applications [3,4]. Readers may refer to a special issue of *IEEE Journal of Oceanic Engineering* on biologically inspired science and technology for autonomous underwater vehicles (AUVs) for excellent review articles and related research [5–9].

Detailed studies have been conducted on fish morphology [4,5,10–13] and locomotion based on which mechanical fins have been designed. Extensive work has been conducted on the measurement of the forces and moments produced by the oscillating fins in various laboratory experiments [10–12,14,15]. Fin movements, such as lead-lag, feathering, and flapping, are identified as the basic oscillating patterns responsible for producing large lift, side force, and thrust, which can be used for the control and propulsion of BAUVs [12,15–17]. Forces and moments associated with the fin movements have also been extracted from computational fluid dynamic (CFD) simulations [18–29], where a number of different fin movement patterns have been considered.

Considerable research has been done for controlling AUVs using traditional control surfaces [31]. A sliding mode control system has been designed for the dive plane control of BAUVs by continuous cambering of dorsal fins [11]. However for fishlike maneuvering, control system design using oscillating fins is essential. Experimental results and CFD simulations of oscillating pectoral fins indicate that these fins produce periodic forces and mo-

ments, and the oscillating parameters (the amplitude of oscillation, frequency, bias angle, phase angle, etc.) can be used as control variables for maneuvering BAUVs [12–14]. Recently, control of AUVs using pectoral fins have been attempted [15–17].

An inverse controller has been designed to maneuver BAUVs in the dive plane using pectoral fins [32]. Although, the characterization of forces and moments generated by oscillating fins, when the chosen control inputs (oscillation parameters) vary in a continuous manner, is important; it seems from literature that this kind of research remains yet to be done. For simplicity, usually numerical simulations using CFD are obtained for a set of fixed oscillation parameters. Thus, for a meaningful utilization of the data obtained using CFD for modeling the forces and moments of the oscillating fins for the purpose of control, it is apparent that the control input (the oscillation parameters) should be changed at discrete intervals only after the completion of a few cycles of the fin motion. Such an attempt to parametrize the forces and moments of a plunging and pitching foil for the dive-plane control of an AUV by switching the bias angle at discrete intervals has been done in [32]. Two-dimensional foil and low Reynolds number flow conditions were chosen for the CFD simulations. The control system designed in [32] is only applicable for the control in the dive plane. Thus, it is of interest to explore the applicability of the pectoral fin control system in the yaw-plane as well. Moreover, the development of parametrizations of the fin forces and moments using new CFD algorithms is certainly desirable for the precision in control.

The contribution of the current paper lies in the parametrization of forces and moments of oscillating pectoral-like fins using CFD; and the design of an optimal control system for the regulation of the yaw angle and an inverse control system for the time-varying yaw trajectory tracking of the AUV. The mechanical foils are assumed to undergo a combined yaw-sway mode of oscillation with the bias angle of the foil as the key control parameter, which is altered at discrete intervals for maneuvering the AUV. For the computation of the fin force and moment, a finite-difference-

¹This work is supported under ONR Grants No. N00014-03-1-0458 and No. N00014-03-1-0897.

Contributed by the Fluids Engineering Division of ASME for publication in the *JOURNAL OF FLUIDS ENGINEERING*. Manuscript received April 8, 2005; final manuscript received December 27, 2005. Assoc. Editor: Ugo Piomelli.

based, Cartesian grid immersed boundary solver for simulating the flow past the flapping foils is used. Three-dimensional foils with finite aspect ratio as well as high Reynolds number flow conditions are chosen in the CFD studies. This makes the simulations more realistic. Moreover, large eddy simulations (LES) are also implemented in current simulations to resolve the turbulence structures. The periodic force and moment obtained using CFD are represented by Fourier series, and a discrete-time AUV model is constructed for the design of two control systems. First, an optimal control law is designed for the control of the yaw (heading) angle by minimizing an appropriate quadratic performance index. The choice of performance criterion gives flexibility in shaping the transient responses. This is followed by the design of an inverse control system for the trajectory control of the yaw angle. It is seen that the number of unstable zeros of the transfer function of the AUV is a function of the position of the pectoral fins on the AUV and the sampling rate. Since the AUV model considered is nonminimum phase, an approximate discrete-time system is obtained by eliminating the unstable zeros from the pulse transfer function of the BAUV. Then an inverse control law is derived for the trajectory tracking based on the approximate minimum phase representation of the transfer function. Simulation results are obtained for the optimal control of the yaw angle and for the tracking of sinusoidal reference yaw angle trajectories using the inverse controller.

The organization of the paper is as follows. Section 2 describes the mathematical model of the BAUV. The CFD-based parametrization and discrete-time representation are obtained in Sec. 3. Sections 4 and 5 present the optimal control law derivation and the inverse controller design, respectively. The simulation results and conclusion are provided in Secs. 6 and 7, respectively.

2 Yaw-Plane Dynamics

Let the vehicle be moving in the yaw plane (X_I - Y_I plane) where $O_I X_I Y_I$ is an inertial coordinate system. $O_B X_B Y_B$ is a body-fixed coordinate system, X_B is in the forward direction, and Y_B points to the right. In the moving coordinate frame $O_B X_B Y_B$ fixed at the vehicle's geometric center, the dynamics for neutrally buoyant vehicle in the yaw plane are given by [33]

$$m(\ddot{v} + Ur + X_G \dot{r} - Y_G r^2) = Y_r \dot{r} + (Y_v \dot{v} + Y_r Ur) + Y_v Uv + F_y$$

$$I_z \dot{r} + m(X_G \dot{v} + X_G Ur + Y_G vr) = N_r \dot{r} + (N_v \dot{v} + N_r Ur) + N_v Uv + M_y$$

$$\dot{\psi} = r \quad (1)$$

where ψ is the heading angle, $r = \dot{\psi}$ is the yaw rate, v is the lateral velocity, $x_{GB} = x_G - x_B$, $y_{GB} = y_G - y_B = 0$, l = body length, ρ = density, m is the mass of the AUV, and I_z is the moment of inertia. Y_v , N_r , Y_r , etc., are the hydrodynamic coefficients. F_y and M_y denote the net lateral (sway) force and yawing moment acting on the vehicle due to the pectoral fins. Here, $((X_B, Y_B) = 0)$ and (X_G, Y_G) denote the coordinates of the center of buoyancy and center of gravity (cg), respectively. Although, the design approach considered in this paper can be used for speed control, here for simplicity, it is assumed that the forward velocity is held steady ($u = U$) by a control mechanism and only lateral maneuvers are considered. In this study, only small maneuvers of the vehicle are considered. As such linearizing the equations of motion about $v = 0$, $r = 0$, $\psi = 0$, one obtains

$$\begin{bmatrix} m - Y_v & mX_G - Y_r & 0 \\ mX_G - N_v & I_z - N_r & 0 \\ 0 & 0 & 1 \end{bmatrix} \begin{bmatrix} \dot{v} \\ \dot{r} \\ \dot{\psi} \end{bmatrix} = \begin{bmatrix} Y_v U & Y_r U - mU & 0 \\ N_v U & N_r U - mX_G U & 0 \\ 0 & 1 & 0 \end{bmatrix} \begin{bmatrix} v \\ r \\ \psi \end{bmatrix} + \begin{bmatrix} F_y \\ M_y \\ 0 \end{bmatrix} \quad (2)$$

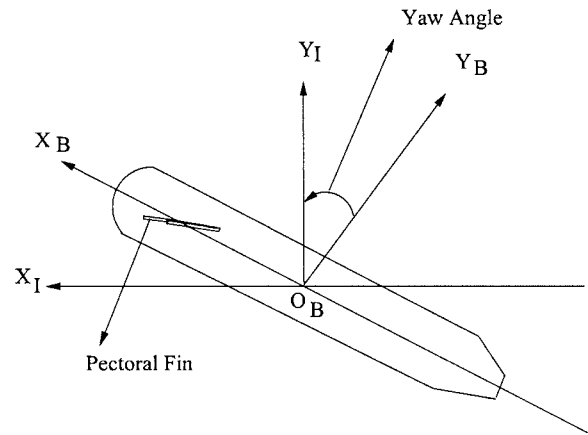


Fig. 1 Model of the underwater vehicle with the pectoral fins

Defining the state vector $x = (v, r, \psi)^T \in R^3$, solving Eq. (2), one obtains a state variable representation of the form

$$\begin{aligned} \dot{x} &= Ax + B_v \begin{bmatrix} F_y \\ M_y \end{bmatrix} \\ y &= [0, 0, 1]x \end{aligned} \quad (3)$$

for appropriate matrices $A \in R^{3 \times 3}$ and $B_v \in R^{3 \times 2}$, where y (heading angle) is the controlled output variable.

We are interested in developing (i) an optimal control system for the heading angle regulation to given set points and (ii) an inverse controller for tracking time-varying reference trajectories, $y_r(t)$.

3 Parametrization Based on CFD and Discrete State Variable Representation

It is assumed that the BAUV model has one pair of pectoral fins that are arranged symmetrically around the body of the AUV. Figure 1 shows a schematic of a typical AUV. Each fin is assumed to undergo a combined sway-yaw motion described as follows:

$$s(t) = s_1 \sin(\omega_f t)$$

$$\theta(t) = \beta + \theta_1 \sin(\omega_f t + \nu_1) \quad (4)$$

where s and θ correspond to the sway and yaw angle of the oscillating fin, respectively. The swaying is assumed to occur about the center-chord location. Furthermore, ω_f , s_1 , and θ_1 are the frequency and amplitudes of oscillations, β is yaw bias angle, and ν_1 is the phase difference between the yawing and swaying motions.

As a result of this flapping motion, each fin experiences a time-varying hydrodynamic force that can be resolved into a sway force component f_y and yawing moment m_y . The pectoral fin can be suitably attached to the vehicle to produce rolling and yawing moments on the BAUV, which affect its dynamics. However, since yaw-plane dynamics and maneuvering is assumed to be affected by the sway force and yawing moment only, we limit our discussion to these components.

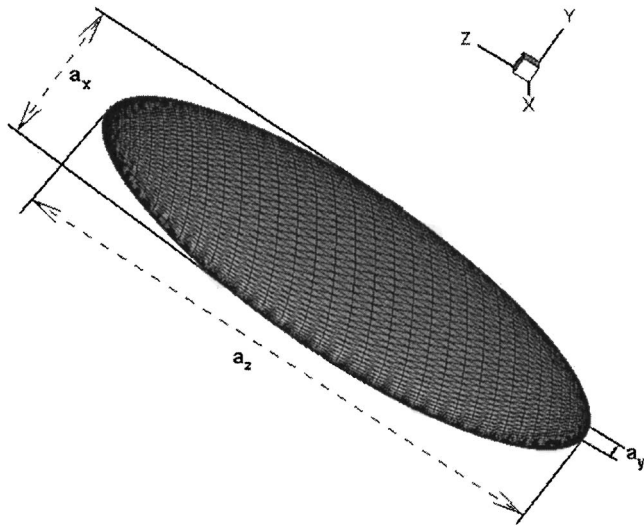


Fig. 2 A thin ellipsoidal foil defined in terms of a surface mesh with triangular elements

Since $f_y(t)$ and $m_y(t)$ produced by each fin are periodic functions, they can be represented by the Fourier series

$$f_y = \sum_{n=0}^N [f_n^s \sin(n\omega_f t) + f_n^c \cos(n\omega_f t)]$$

$$m_y = \sum_{n=0}^N [m_n^s \sin(n\omega_f t) + m_n^c \cos(n\omega_f t)]$$
(5)

where it is assumed that the fins produce dominant N harmonically related components and the harmonics of higher frequencies are negligible. The Fourier coefficients f_n^a and m_n^a , $a \in \{s, c\}$, capture the characteristics of the time-varying signals $f_y(t)$ and $m_y(t)$. Parametrization of these coefficients is therefore needed in order to complete the equations that govern the motion of the BAUV in the yaw plane.

3.1 CFD Based Parametrization. A finite-difference-based, Cartesian grid immersed boundary solver [22] has been used to simulate the flow past flapping foils in the current study. The key feature of this method is that simulations with complex moving bodies can be carried out on stationary nonbody conformal Cartesian grids, and this eliminates the need for complicated remeshing algorithms that are usually employed with conventional Lagrangian body-conformal methods. The Eulerian form of the incompressible Navier-Stokes equations is discretized on a Cartesian mesh and boundary conditions on the immersed boundary are imposed through a “ghost-cell” procedure [19]. The method employs a second-order center-difference scheme in space and a second-order accurate fractional-step method for time advancement. The code employs the large-eddy simulation (LES) approach in order to account for the effect of the small subgrid flow scales on the large resolved scales. A Lagrangian dynamic model [27] is used to estimate the subgrid-scale eddy viscosity. The details of the numerical method and validation of the code can be found in [28].

Thin ellipsoidal foils are employed in the current study. The geometry of the foil is defined by its three major axes denoted by a_x , a_y , and a_z , as shown in Fig. 2. The surface of the foil is represented by a fine, unstructured mesh with triangular elements. Note that the foil is oriented with the x -axis along the streamwise direction and the z -axis along the spanwise direction. Furthermore, a_x is also the chord of the foil, which in these simulations is set equal to unity, and a_y is the foil thickness. The ratio a_y/a_x and

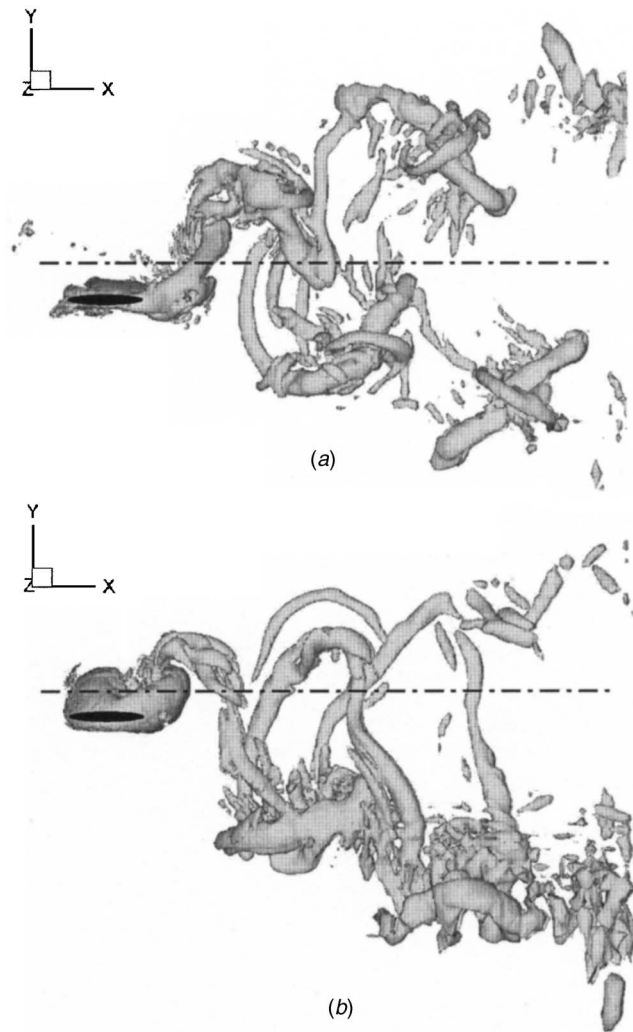


Fig. 3 Side view of wake structures for flow past the flapping foil with two yaw-bias angles: (a) bias angle 0 deg and (b) bias angle 20 deg

a_z/a_x in the current study is equal to 0.12 and 2.0, respectively. In addition to these foil geometric parameters, the following are the other key nondimensional parameters in the current study: Reynolds number $Re = U_\infty a_x / \nu$; normalized sway amplitude s_1/a_x , yaw-bias angle β , yaw amplitude θ_1 , phase advance of yawing over swaying ψ_1 , and Strouhal number based on the wake thickness $St = s_1 \omega_f / U_\infty \pi$. In the current simulations, Reynolds number, s_1/a_x , ψ_1 , ν_1 , and St are fixed at value equal to 1000, 0.5, 30 deg, 90 deg, and 0.6, respectively. The yaw-bias angle, β which is the main control parameter, is varied from 0 deg to 20 deg. A nonuniform $177 \times 129 \times 105$ Cartesian mesh is employed in the simulations where the grid is clustered in the region around the flapping foil and in the foil wake. The size of computational domain as well as the number of grids have been chosen so as to ensure the simulation accuracy.

In the current study, the sway force coefficient and moment coefficient are defined as

$$C_Y = \frac{f_y}{\frac{1}{2} \rho U_\infty^2 A_{\text{plan}}}$$
(6)

$$C_M = \frac{m_y}{\frac{1}{2} \rho U_\infty^2 A_{\text{plan}} a_x}$$

where f_y and m_y are the sway force and yawing moment, respectively, and A_{plan} is the projected area of the foil which is equal to

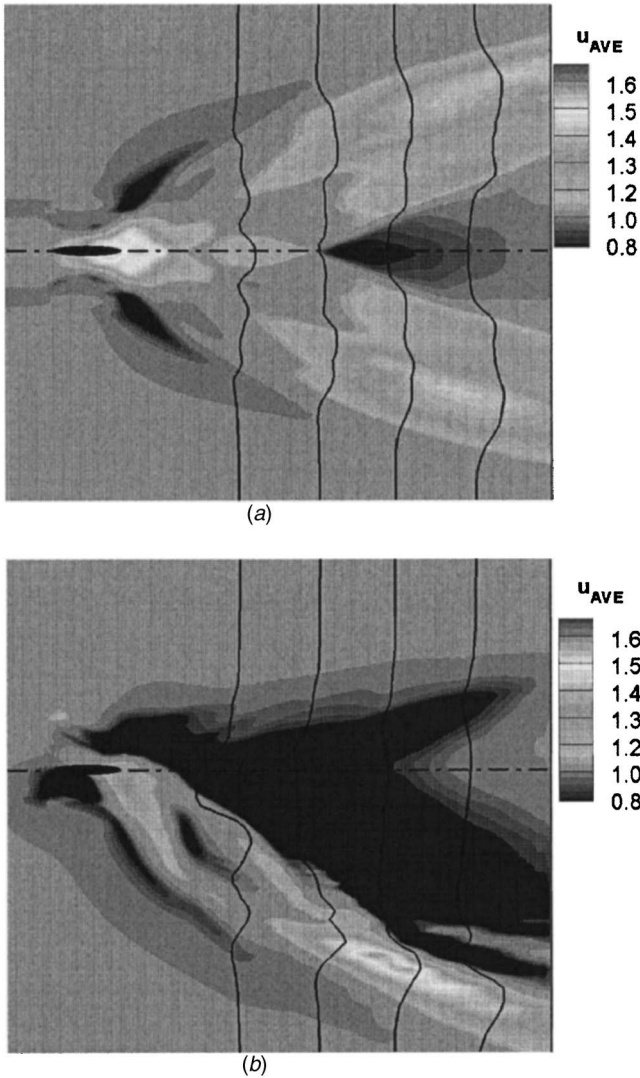


Fig. 4 Center-plane time-averaged streamwise velocity contours for flow past the flapping foil with two yaw-bias angles. Black lines are the streamwise velocity profiles: (a) bias angle 0 deg and (b) bias angle 20 deg

$(\pi/4)a_x a_z$ for the ellipsoidal foils. Forces and moments are calculated by directly integrating the computed pressure and shear stress on the foil surface.

The side views of wake topologies of a yawing-swaying flapping foil with different yaw bias angles, $\beta=0$ deg and 20 deg, are shown in Fig. 3. The isosurfaces of the eigenvalue imaginary part of the velocity gradient tensor of the flow are plotted in order to clearly show the vortex topology [30]. The key feature observed in Fig. 3(a) is the presence of two sets of interconnected vortex loops that slowly convert into vortex rings as they convect downstream in the case of $\beta=0$ deg. The jets formed by these two set of rings contribute equally to the thrust production of the flapping foil, and zero mean sway force is expected. As seen in Fig. 3(b), when yaw-bias angle increases, one of those two sets of vortex rings becomes weaker and the other one grows. This asymmetry is associated with the production of a mean sway-force on the fin. Figure 4 shows the time-averaged streamwise velocity contours for both of these cases. For the $\beta=0$ deg foil, two oblique jets with equal strength are observed. As yaw-bias angle increases, the lower jet becomes stronger while the upper jet essentially disappears. As a result of this, the sway force is modified significantly. Table 1 shows the changes in the mean sway force coefficients

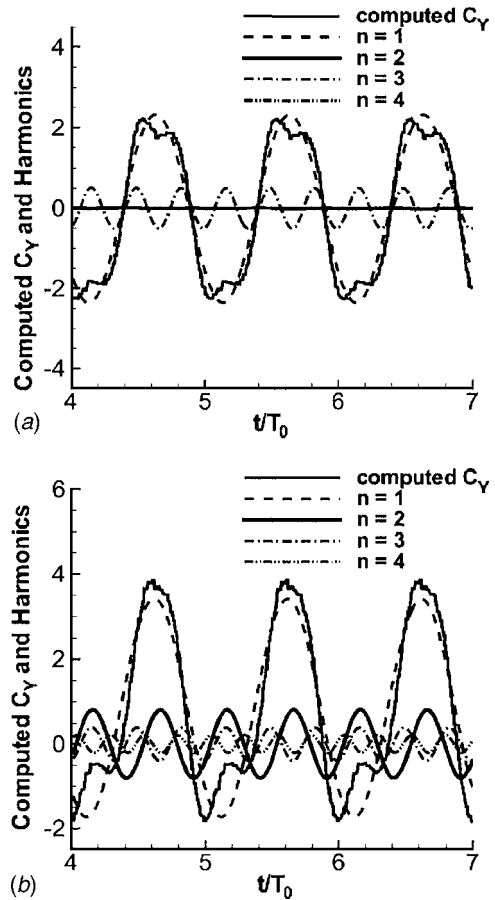


Fig. 5 Harmonic components of the force for two yaw-bias angles: (a) bias angle 0 deg and (b) bias angle 20 deg

and the mean yawing moment coefficients for different bias angles. It can be seen that small changes in the yaw-bias angle can produce large changes in the mean sway force as well as the yawing moment. This clearly suggests that the yaw-bias angle is an effective control parameter for precise maneuvering.

We assume that the bias-angle (control input) β is varied at discrete intervals and the remaining oscillation parameters are kept constant. The current simulations (Table 1) indicates that the sway force and yawing moment are nearly linear with yawing-bias angle β over a large range of this parameter. Similar variation in mean lateral force with bias angle has been noted in experiments [13,14] and simulations of two-dimensional (2D) pitching-heaving foils [29].

Expanding the fin force and moment of each fin in a Taylor series about $\beta=0$ gives

$$f_y(t, \beta) = f_y(t, 0) + \frac{\partial f_y}{\partial \beta}(t, 0)\beta + O(\beta^2) \quad (7)$$

$$m_y(t, \beta) = m_y(t, 0) + \frac{\partial m_y}{\partial \beta}(t, 0)\beta + O(\beta^2)$$

where $O(\beta^2)$ denotes higher-order terms. We assume here that for a fixed $\beta \in R$, $f_y(t+T_0, \beta) = f_y(t, \beta)$ and $m_y(t+T_0, \beta) = m_y(t, \beta)$, t

Table 1 C_Y and C_M for different yaw-bias angles

Yaw-bias angle (deg)	C_Y	C_M
0	0.00	0.00
10	1.52	-0.14
20	2.74	-0.26

Table 2 Table showing various components of force and moment coefficient for the $\beta_y=0$ deg case

n	f_n^c	f_n^s	m_n^c	m_n^s
0	0.00	0.00	0.00	0.00
1	-5.62	-5.16	0.90	1.11
2	0.08	-0.05	-0.01	0.00
3	-1.31	0.8	-0.17	0.00
4	0.09	-0.02	-0.01	0.01

>0 (T_0 denotes the fundamental period). Then, the partial derivatives of f_y and m_y with respect to β are also periodic functions of time. Using Eq. (7), one can approximately express f_y and m_y as

$$\begin{aligned}
 f_y &= \sum_{n=0}^N f_n^s(0) \sin nw_{ft} + f_n^c(0) \cos nw_{ft} \\
 &+ \sum_{n=0}^N \left[\frac{\partial f_n^s}{\partial \beta}(0) \sin nw_{ft} + \frac{\partial f_n^c}{\partial \beta}(0) \cos nw_{ft} \right] \beta \\
 m_y &= \sum_{n=0}^N m_n^s(0) \sin nw_{ft} + m_n^c(0) \cos nw_{ft} \\
 &+ \sum_{n=0}^N \left[\frac{\partial m_n^s}{\partial \beta}(0) \sin nw_{ft} + \frac{\partial m_n^c}{\partial \beta}(0) \cos nw_{ft} \right] \beta
 \end{aligned} \tag{8}$$

where $O(\beta^2)$ terms are ignored in the series expansion.

Thus, we get

$$\begin{aligned}
 f_y(t) &= \phi^T(f_a + \beta f_b) \\
 m_y(t) &= \phi^T(m_a + \beta m_b)
 \end{aligned} \tag{9}$$

$$\phi = [1 \sin w_{ft} \dots \sin Nw_{ft} \cos Nw_{ft}]^T$$

where $f_a, f_b, m_a, m_b \in R^{2N+1}$ and can be obtained from Eq. (8).

Thus, in order to complete the equations that govern the motion of the BAUV in the yaw plane, the Fourier components of the force are needed. Figure 5 shows the dimensionless time variation of computed mean sway force coefficient and its harmonic components for yaw bias angles of 0 deg and 20 deg, respectively. Note the even modes ($n=2, 4$) for the zero bias angle have negligible contribution to the fin force. It is also seen that fin force of larger magnitude is obtained when the bias angle is increased. Furthermore, the amplitudes of higher harmonics diminish as n increases. Tables 2 and 3 show both the force and moment Fourier coefficients for the yaw bias of 0 deg and 20 deg for different harmonics (see Eq. (8)). It is seen from the tables that the Fourier coefficients of the fourth harmonic are quite small compared to the coefficients of the first harmonic. As such, even four harmonic components are sufficient to capture most of the characteristics of the time-varying signals $f_y(t)$ and $m_y(t)$.

3.2 Discrete Time State Variable Representation. The vehicle has two attached fins; therefore, the net force and moment

Table 3 Table showing various components of force and moment coefficient for the $\beta_y=20$ deg case

n	f_n^c	f_n^s	m_n^c	m_n^s
0	2.74	0.00	-0.26	0.00
1	-6.75	-4.98	0.75	0.65
2	-0.68	2.54	0.01	-0.14
3	-1.1	0.63	-0.13	0.04
4	0.15	0.14	-0.03	0.04

are $F_y=2f_y$ and $M_y=2(d_{cgf}f_y+m_y)$, where d_{cgf} is the moment arm due to the fin location (positive forward). Using Eq. (9), the yaw-plane dynamics Eq. (3) can be written as

$$\dot{x} = Ax + B\Phi(t)f_c + B\Phi(t)f_v\beta \tag{10}$$

where $B[f_y, m_y]^T = B_v[F_y, M_y]^T$, $f_c = (f_a^T, m_a^T)^T \in R^{4N+2}$, and $f_v = (f_b^T, m_b^T)^T \in R^{4N+2}$ where

$$\Phi(t) = \begin{bmatrix} \phi^T(t) & 0 \\ 0 & \phi^T(t) \end{bmatrix} \tag{11}$$

For the purpose of control, the bias angle is changed at a discrete interval of T^* , where T^* is an integer multiple of the period T_0 , i.e., $T^* = n_0 T_0$, where n_0 is a positive integer. This way one switches the bias angle at a uniform rate of T^* seconds at the end of n_0 cycles. For the derivation of the control law, the transients introduced due to changes in the bias-angle are ignored. Since the bias angle switches at discrete intervals, it will be convenient to express the continuous-time system Eq. (10) as a discrete-time system. The function $\beta(t)$ now has piecewise constant values β_k for $t \in [kT^*, (k+1)T^*]$, $k=0, 1, 2, \dots$

Discretizing the state equation (10), one obtains a discrete-time representation of the form

$$x[(k+1)T^*] = A_d x(kT^*) + B_d \beta_k + d \tag{12}$$

where $A_d = e^{AT^*}$, $B_d = \int_0^{T^*} e^{As} B \Phi(-s) ds$, $B_d = B_0 f_v \in R^3$, and $d = B_0 f_c \in R^3$.

The output variable (y) is

$$y(kT^*) = [0 \ 0 \ 1] x(kT^*) = C_d x(kT^*) \tag{13}$$

4 Optimal Yaw-Plane Control

In this section, the design of an optimal feedback yaw-plane control law for the regulation of the yaw angle is considered. For the precise yaw control, it is desirable to include a feedback term in the control law that is proportional to the integral of the yaw tracking error. For this purpose, a new state variable x_s is introduced that satisfies

$$\dot{x}_s[(k+1)T^*] = \psi^* - y(kT^*) + x_s(kT^*) \tag{14}$$

where ψ^* , a constant, is the desired yaw angle and $\psi^* - y(kT^*)$ is the tracking error.

Defining the state vector $x_a = (x^T, x_s)^T \in R^4$ and using Eqs. (12) and (14), the augmented system takes the form

$$\begin{aligned}
 x_a[(k+1)T^*] &= \begin{bmatrix} A_d & 0 \\ -C_d & 1 \end{bmatrix} \begin{bmatrix} x(kT^*) \\ x_s(kT^*) \end{bmatrix} + \begin{bmatrix} B_d \\ 0 \end{bmatrix} \beta_k + \begin{bmatrix} d \\ \psi^* \end{bmatrix} \\
 &= A_a x_a(kT^*) + B_a \beta_k + d_a
 \end{aligned} \tag{15}$$

where the constant matrices A_a , B_a , and d_a are defined in Eq. (15).

The control of the system, Eq. (15) can be accomplished by following the servomechanism design approach [34] in which d_a is treated as a constant disturbance input. The design is completed by computing a feedback control law of the form

$$\beta(kT^*) = -\mathbf{K} x_a(kT^*), k=0, 1, 2, \dots \tag{16}$$

where \mathbf{K} is a constant row vector such that the closed-loop matrix

$$A_c = (A_a - B_a \mathbf{K})$$

is stable. It is well known that one can assign the eigenvalues of A_c arbitrarily if (A_a, B_a) is controllable [35,36]. For the discrete-time system, this implies that one must choose \mathbf{K} such that the eigenvalues of A_c are strictly within the unit disk in the complex plane.

In this study, an appropriate value of \mathbf{K} is obtained by using the linear quadratic optimal control theory [35]. For this, one chooses a performance index of the form

$$J_o = \sum_{k=0}^{\infty} x_a^T(kT^*) Q x_a(kT^*) + \beta_k^2 \mu \quad (17)$$

where Q is a positive definite symmetric matrix and $\mu > 0$. The weighting matrix Q associated with x_a and the parameter μ penalizing the level of the bias angle are chosen to provide a trade-off between the convergence rate of the state variables to the equilibrium point and the bias angle magnitude.

The optimal control law is obtained by minimizing J_o for the system

$$x_a[(k+1)T^*] = A_a x(kT^*) + B_a \beta_k \quad (18)$$

which is obtained from Eq. (15) by setting $d_a=0$. The feedback matrix K is obtained by solving the discrete Riccati equation [35]

$$P = Q + A_a^T P A_a - A_a^T P B_a (\mu + B_a^T P B_a)^{-1} B_a^T P A_a \quad (19)$$

and then setting the feedback matrix as

$$K = -(\mu + B_a^T P B_a)^{-1} B_a^T P A_a \quad (20)$$

Using the feedback law Eq. (16), the yaw angle can be regulated to prescribed constant values ψ^* , but the BAUV cannot follow time-varying yaw angle trajectories. In Sec. (6), an inverse control law is derived for the tracking of time-varying trajectories.

5 Inverse Control System

The transfer function relating the output $y(kT^*)$ and the input β_k of Eq. (12) (assuming that $d=0$) is given by

$$\frac{\hat{y}(z)}{\hat{\beta}(z)} = G(z) = C_d(zI - A_d)^{-1} B_d = k_p \frac{(z + \mu_1)(z + \mu_2)}{z^3 + a_2 z^2 + a_1 z + a_0} \quad (21)$$

where z denotes the Z-transform variable, $\mu_i (i=1,2)$ are real or complex numbers, and k_p and $a_i (i=0,1,2)$ are real numbers. It is assumed that the pectoral fins are attached between the cg and the nose of the vehicle. For the AUV model under consideration, the number of unstable zeros (i.e., the zeros outside the unit disk in the complex plane) depend on the distance (d_{cgf}) of the pectoral fins from the cg, ω_f , and the sampling time T^* . It has been found that for the values of interest of the oscillation frequencies and the attachment point (d_{cgf}) of the fins, there exists a single unstable zero (i.e., the transfer function is nonminimum phase).

It is well known that the inverse control design can be accomplished only when the system is minimum phase (i.e., the zeros of the transfer function are stable). For this purpose, the original transfer function is simplified by ignoring its unstable zero. Let us assume that $\mu_1 > 1$ and $\mu_2 < 1$. For obtaining a minimum phase approximate system, one removes the unstable zero of $G(z)$ but retains the zero frequency (dc) gain. Thus the approximate transfer function $G_a(z)$ obtained from Eq. (21) takes the form

$$G_a(z) = k_p \frac{(1 + \mu_1)(z + \mu_2)}{\Delta(z)} \quad (22)$$

where $\Delta(z) = \det(zI - A_d)$.

We are interested in deriving a new controlled output variable y_a such that

$$y_a(kT^*) = C_a x(kT^*) \quad (23)$$

$$\frac{\hat{y}_a(z)}{\hat{\beta}(z)} = G_a(z) = C_a(zI_n - A_d)^{-1} B_d \quad (24)$$

where C_a is a new output matrix. Since the relative degree of $G_a(z)$ is 2, one has

$$C_a B_d = 0$$

$$C_a A_d B_d \neq 0 \quad (25)$$

Using the Leverrier algorithm, the approximate transfer function $G_a(z)$ can be expanded as [35]

$$G_a(z) = \Delta^{-1}(z) [(z + a_2) C_a A_d B_d + C_a A_d^2 B_d] \quad (26)$$

Comparing Eqs. (21) and (25), one can easily show that

$$C_a [B_d A_d B_d A_d^2 B_d + a_2 A_d B_d] = [0 \ K_p(1 + \mu_1) \ K_p(1 + \mu_1)\mu_2] \quad (27)$$

Solving Eq. (27), one obtains the modified output matrix.

For the modified system, one has

$$x[(k+1)T^*] = A_d x(kT^*) + B_d \beta_k + d \quad (28)$$

$$y_a(kT^*) = C_a x(kT^*)$$

Suppose a reference trajectory $y_r(kT^*)$ is given that is to be tracked by $y_a(kT^*)$. Using Eq. (28), one has that

$$y_a[(k+1)T^*] = C_a A_d x(kT^*) + C_a d \quad (29)$$

$$y_a[(k+2)T^*] = C_a A_d^2 x(kT^*) + \sum_{i=0}^1 C_a A_d^i d + C_a A_d^{(r-1)} B_d \beta_k$$

In view of Eq. (29), for following the reference trajectory $y_r(kT^*)$, we choose the control input β_k as

$$\beta_k = (C_a A_d B_d)^{-1} \left[-C_a A_d^2 x(kT^*) - \sum_{i=0}^1 C_a A_d^i d + v_k \right] \quad (30)$$

where the signal v_k is selected as

$$v_k = y_r[(k+2)T^*] - p_1 \{C_a A_d x(kT^*) + C_a d - Y_r[(k+1)T^*]\} + p_0 [Y_a(kT^*) - Y_r(kT^*)] \quad (31)$$

where p_0 and p_1 are real numbers.

Defining the tracking error $e(kT^*) = y_a(kT^*) - y_r(kT^*)$ and using the control law Eqs. (30) and (31) in Eq. (29) gives

$$e[(k+2)T^*] + p_1 e[(k+1)T^*] + p_0 e(kT^*) = 0 \quad (32)$$

The tracking error equation (32) satisfies a second-order difference equation. The characteristic polynomial associated with Eq. (32) is

$$(z^2 + p_1 z + p_0) = 0 \quad (33)$$

The parameters p_i are chosen such that the roots of Eq. (33) are strictly within the unit disk. Then it follows that for any initial condition $x(0), e(kT^*) \rightarrow 0$ as $k \rightarrow \infty$ and the controlled output $y_a(kT^*)$ asymptotically converges to the reference sequence $y_r(kT^*)$. In Sec. 6, it will be seen that the inverse controller designed based on the approximate transfer function accomplishes accurate yaw angle trajectory control. This completes the inverse controller design.

6 Simulation Results for Yaw Maneuvers

In this section, simulation results using the MATLAB/SIMULINK software is presented. The performance of the optimal and inverse controllers for different values of frequencies of oscillation of the pectoral fin and for different points of attachment of the fins to the BAUV (d_{cgf}) from the center of gravity of the AUV is examined.

The parameters of the model are taken from [33]. The AUV is assumed to move with a constant forward velocity of 0.7 m/s with the help of a control mechanism. The vehicle parameters are $l=1.391$ m, $mass=18.826$ kg, $I_z=1.77$ kgm², $X_G=-0.012$, $Y_G=0$. The hydrodynamic parameters for a forward velocity of 0.7 m/s derived from [33] are $Y_{\dot{\psi}}=-0.3781$, $Y_{\dot{\psi}}=-5.6198$, $Y_{\psi}=1.1694$, $Y_v=-12.0868$, $N_{\dot{\psi}}=-0.3781$, $N_{\dot{\psi}}=-0.8967$, $N_{\psi}=-1.0186$, and $N_v=-4.9587$.

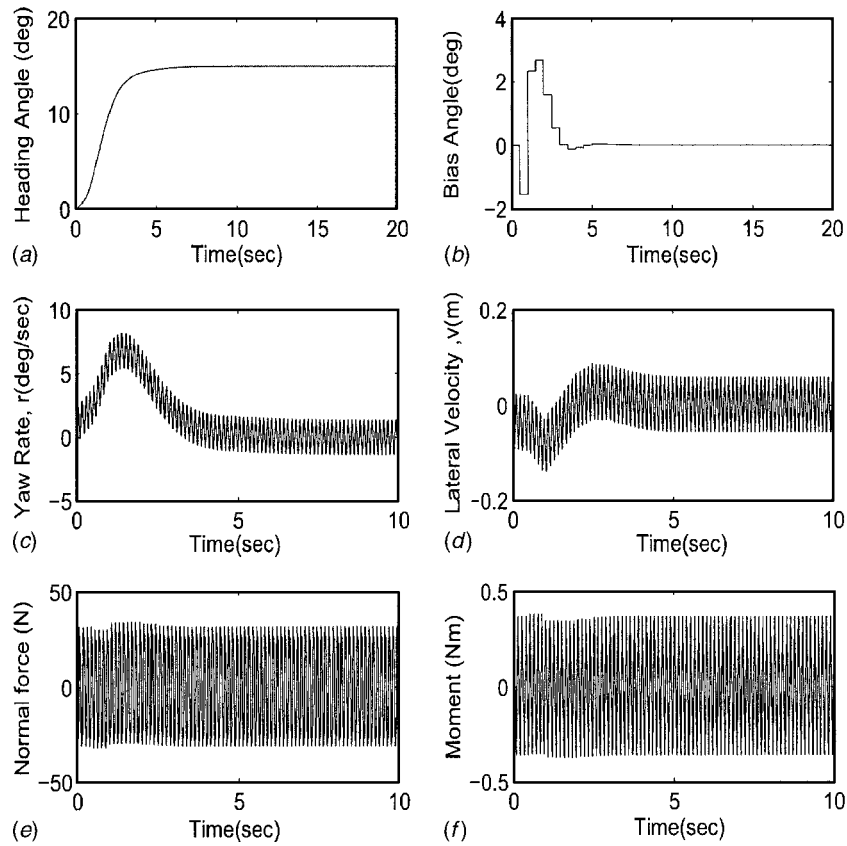


Fig. 6 Optimal control: Frequency of flapping=8 Hz, $d_{cgf}=0$ m for $\psi^*=15$ deg: (a) heading angle, ψ (deg); (b) bias angle (control input), β (deg); (c) yaw rate, r (deg/s); (d) lateral velocity, v (m/s); (e) lateral force, F_y (N); and (f) side moment, M_y (Nm)

Experimental results indicate that for zero bias angle, the mean values of f_y and m_y are nearly zero. Therefore, the vectors f_a , f_b , m_a , and m_b are found to be

$$f_a = (0, -40.0893, -43.6632, -0.3885, 0.6215, 6.2154, -10.17, -0.1554, 0.6992)$$

$$f_b = (68.9975, 0.4451, -16.4704, 64.1009, -19.5864, -0.8903, -2.2257, 2.2257, 4.8966)$$

$$m_a = (0.0054, 0.6037, 0.4895, 0, -0.0054, 0, -0.0925, 0, -0.0054)$$

$$m_b = (-0.5297, -0.3739, -0.0935, -0.2493, 0.1246, 0.0312, -0.0312, 0.0935, 0)$$

It is pointed out that these parameters are obtained from the force and moment Fourier coefficients and are computed by multiplying the Fourier coefficients by $(1/2)\rho \cdot W_a \cdot U_\infty^2$ and $(1/2)\rho \cdot W_a \cdot \text{chord} \cdot U_\infty^2$, respectively, where W_a is the surface area of the foil. For simulation, the initial conditions of the vehicle are assumed to be $x(0)=0$ and $x_s(0)=0$.

6.1 Optimal Yaw-Plane Control. In this section, the feedback discrete control law Eq. (16) is simulated. The bias angle is changed to a new value every $T^* = n_0 T_0$ seconds where $T_0 = 1/f_0$ is the fundamental period of f_p and m_p . Choosing a small value of n_0 increases the transients produced due to switching. Parametrization of these transients is quite difficult since they introduce a number of additional parameters into the problem. On the other hand, a large value of n_0 increases the magnitude of the inter-

sample oscillations, which is also not desirable.

The terminal state is chosen as $x^* = (0, 0, 15)^T$ with $\psi^* = 15$ deg. Thus, one desires to control the BAUV to a heading angle of 15 deg. For optimal control design, the weighting matrix and parameter are selected as $Q = 1000I_{4 \times 4}$ and $\mu = 1.5$. Simulation results are provided for fin frequencies of 8 Hz and 6 Hz.

Case 1. Optimal Control: Frequency of Fin Oscillation 8 Hz, $d_{cgf}=0$ and $d_{cgf}=0.15$ (m). First simulation is done for the higher frequency of 8 Hz and the fin attachment point is chosen such that $d_{cgf}=0$. Note that with this value of d_{cgf} , the sway force itself does not produce any yawing moment on the BAUV. The control law is updated every four cycles, i.e., $T^* = 4T_0 = 0.5$ s. The value of $n_0 = 4$ is found to be an appropriate compromise between minimizing transients and intersample oscillations. The transfer function $G(z)$ has a stable zero at 0.0965 and an unstable zero at -1.5548 . As such $G(z)$ is minimum phase. Figure 6 shows the simulated results. It can be seen that the optimal controller achieves accurate heading angle control to the target set point in ~ 5 s. The control input (bias angle) magnitude required is < 3 deg, which is small and can easily be provided by the pectoral fins. The plots of the lateral force and moment produced by the fins are also provided in the figure. In the steady state, the lateral fin force and moment exhibit bounded periodic oscillations. The intersample yaw angle shows oscillations of tiny amplitude, however, in the terminal phase, the sample values of yaw angle is equal to the commanded value ψ^* .

Simulation results for the same frequency, but for a d_{cgf} value of 0.15 m are also presented (Fig. 7). Note that with a nonzero value of d_{cgf} , the sway force also produces additional yawing

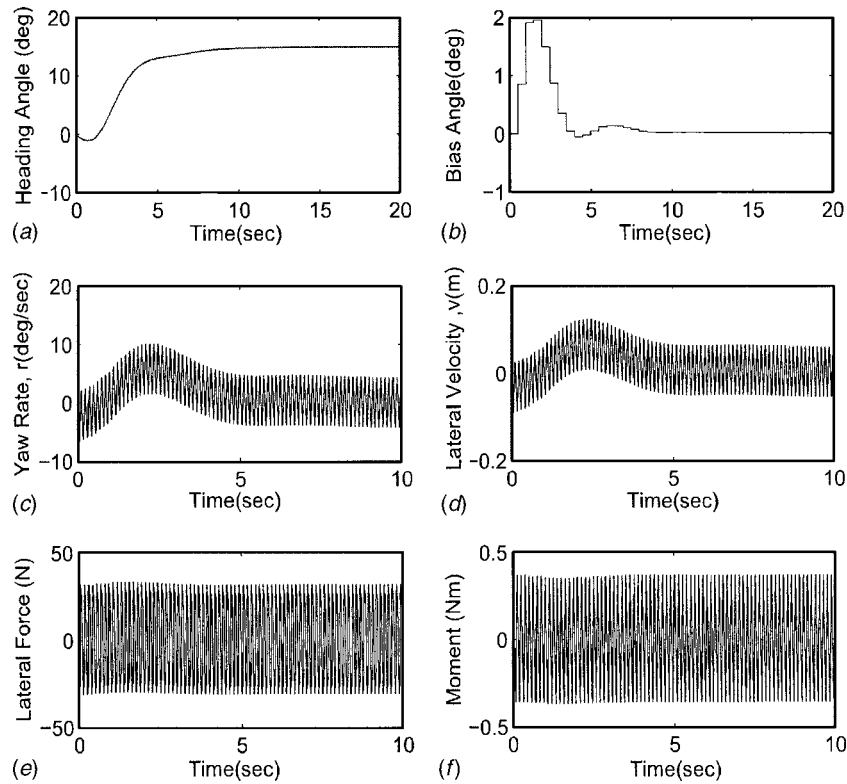


Fig. 7 Optimal control: Frequency of flapping=8 Hz, $d_{cgf}=0.15$ m for $\psi^*=15$ deg: (a) heading angle, ψ (deg); (b) bias angle (Control input), β (deg); (c) yaw rate, r (deg/s); (d) lateral velocity, v (m/s); (e) lateral force, F_y (N); and (f) side moment, M_y (Nm)

moment on the BAUV. Unlike the previous case, the zeros of $G(z)$ are now at 1.48 and -0.75 . It is seen that the stable zero at 0.0965 of the model for $d_{cgf}=0$ has moved to a lesser stable position at -0.75 in the unit disk for the model with $d_{cgf}=0.15$ m. The transient response for $d_{cgf}=0.15$ m is not as good as in Fig. 6, and the settling time is larger. It is also observed that, initially, the vehicle heading angle swings in the wrong direction, but the target yaw angle is attained in the steady state.

Case 2. Optimal control: Frequency of Oscillation 6 Hz, $d_{cgf}=0$ and $d_{cgf}=0.15$ (m). This simulation is done for a lower value of fin frequency of 6 Hz with a d_{cgf} value of 0. The sampling period T^* is still kept equal to $4T_0$, which for this case is equal to $2/3$ s. Thus, compared to the case of 8 Hz, the control is updated at a slower rate. The zeros of $G(z)$ are at -1.6813 and 0.0331 . The simulation results are shown in Fig. 8. One can observe that the yaw angle control is accomplished; however, intersample oscillations of larger magnitude compared to Fig. 6 are present. This is an expected phenomenon because the bias angle switches after a longer period, but the convergence time of the yaw angle is found to be almost the same. The maximum magnitude of control input required for the maneuver is also larger, and the sway force and moment were found to be less than 60 N and 1 Nm, respectively.

Simulation for a d_{cgf} value of 0.15 m was also performed at this frequency, and the results are shown in Fig. 9. In this case, it is found that the zeros (1.7138, -0.7058) of $G(z)$ have moved away from the origin compared to the model for $d_{cgf}=0$. It is observed that although the heading angle is controlled, the magnitude of the intersample oscillations has increased.

6.2 Inverse Yaw-Plane Control. For the tracking of time-varying reference trajectories, the designed inverse control system is suitable. In this subsection, simulation results for sinusoidal heading angle trajectory tracking for different fin-flapping fre-

quencies are presented. Smooth sinusoidal reference trajectories are generated by command generators of the form

$$(E^3 + p_{c2}E^2 + p_{c1}E + p_{c0})y_r(kT^*) = (1 + p_{c0} + p_{c1} + p_{c2}) \times d^* \sin(w_r kT^*)$$

where E denotes the advance operator ($E y_r(kT^*) = y_r[(k+1)T^*]$) and d^* is the amplitude of the sine wave and the parameters p_{ci} are chosen to be zero so that the poles of the command generator are at $z=0$. The reference trajectory generator is simulated using its state variable form with states $x_r = (x_{r1}, x_{r2}, x_{r3})^T$. For the simulation, $d^* = 15$ deg and $w_r = 0.2$ rad/s.

Simulation results for fin frequencies of 8 Hz and 6 Hz are presented in the following subsection.

Case 3. Inverse control: Frequency of Oscillation 8 Hz, $d_{cgf}=0$ and $d_{cgf}=0.15$ (m). Figure 10 shows the inverse controller performance for a $d_{cgf}=0$. The sampling period is $4T^* = 1/2$. It can be observed that smooth heading angle trajectory control is achieved. One can observe that the modified output equals the reference trajectory at all sample instants. The maximum control input (bias angle) required is ~ 3 deg. The lateral force and moment produced by the fins are less than 40 N and 0.4 Nm, respectively. As expected, the yaw rate and the lateral velocity are sinusoidal.

Simulation are also done for $d_{cgf}=0.15$ m. The plots are shown in Fig. 11. Although the heading angle tries to follow the command trajectory, in the initial period, the yaw angle trajectory is not smooth and there is a larger tracking error compared to Fig. 10. For $d_{cgf}=0$, the tracking performance is extremely good as seen in Fig. 10. The performance of the inverse controller for time-varying trajectory tracking for nonzero d_{cgf} deteriorates because the zero dynamics (the residual dynamics) for d_{cgf}

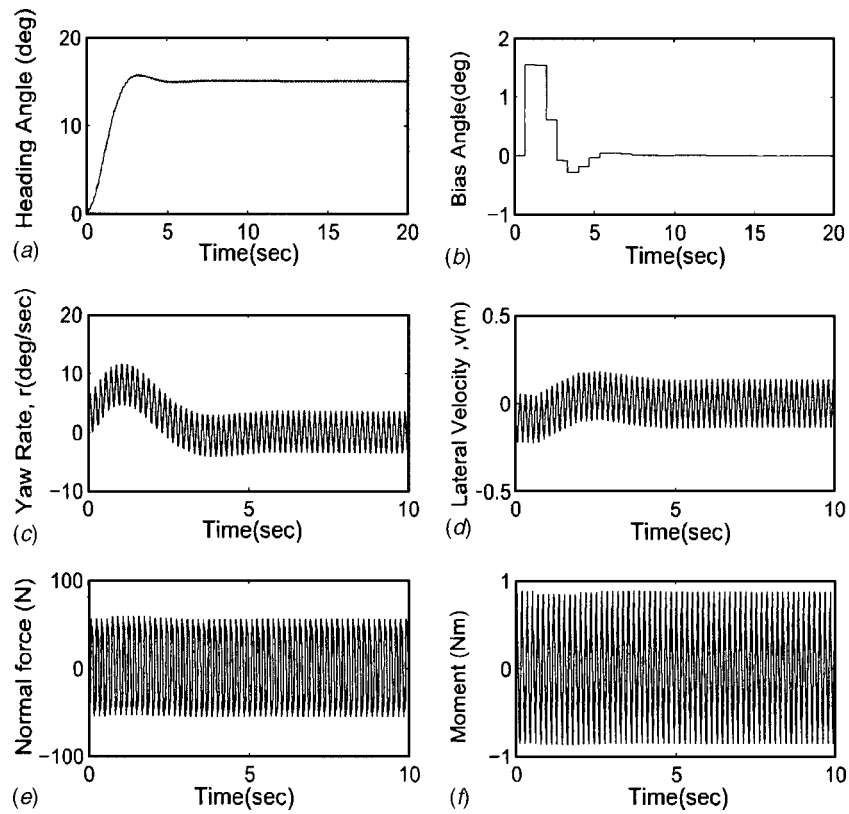


Fig. 8 Optimal control: Frequency of flapping=6 Hz, $d_{cgf}=0$ m for $\psi^* = 15$ deg: (a) heading angle, ψ (deg); (b) bias angle (control input), β (deg); (c) yaw rate, r (deg/s); (d) lateral velocity, v (m/s); (e) lateral force, F_y (N); and (f) side moment, M_y (Nm)

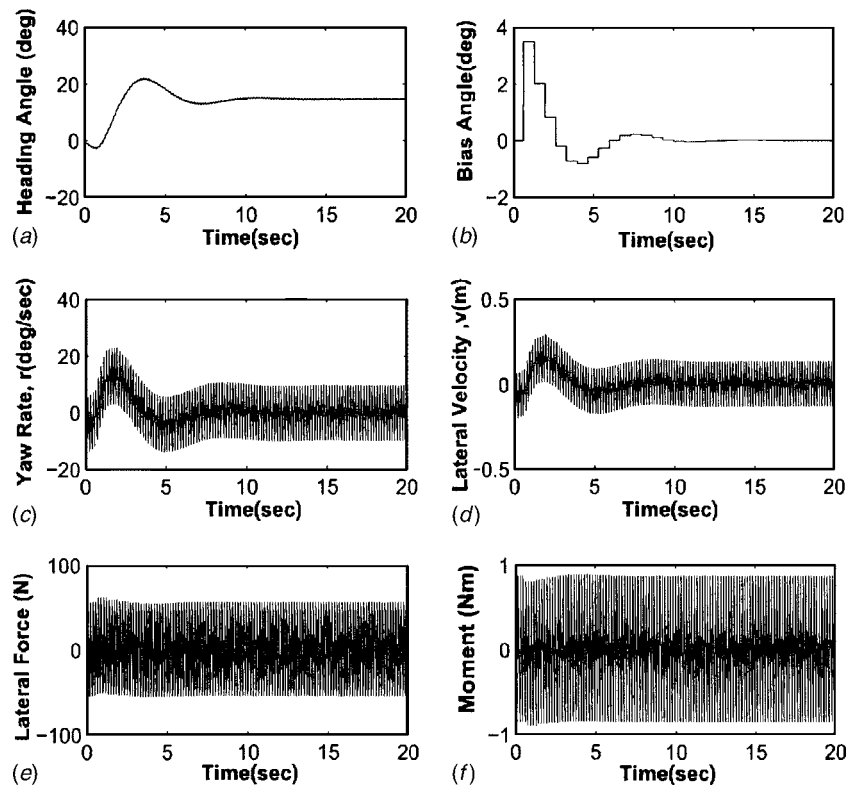


Fig. 9 Optimal control: Frequency of flapping=6 Hz, $d_{cgf}=0.15$ m for $\psi^* = 15$ deg: (a) heading angle, ψ (deg); (b) bias angle (control input), β (deg); (c) yaw rate, r (deg/s); (d) lateral velocity, v (m/s); (e) lateral force, F_y (N); and (f) side moment, M_y (Nm)

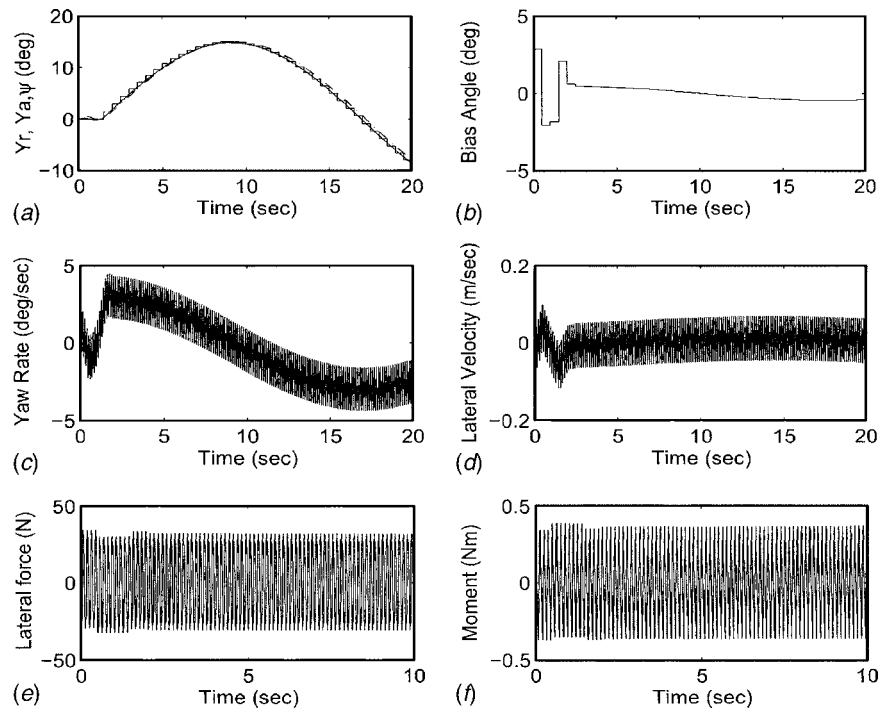


Fig. 10 Inverse control: Frequency of flapping=8 Hz, $d_{cgr}=0$ m for $\psi^* = 15$ deg: (a) reference heading angle, Y_r (staircase); modified heading angle Y_a (broken line); and actual heading angle ψ (solid line) (deg); (b) Bias angle (control input), β (deg); (c) yaw rate, r (deg/s); (d) lateral velocity, v (m/s); (e) lateral force, F_y (N); and (f) side moment, M_y (Nm).

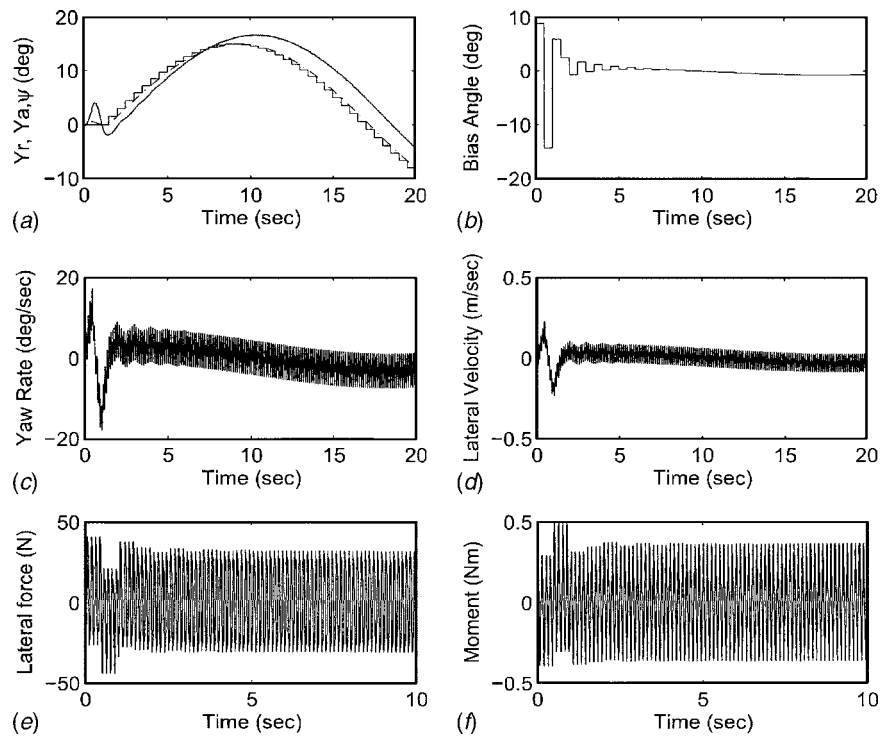


Fig. 11 Inverse control: Frequency of flapping=8 Hz, $d_{cgr}=0.15$ m for $\psi^* = 15$ deg: (a) reference heading angle, Y_r (staircase); modified heading angle, Y_a (broken line); and actual heading angle, ψ (solid line) (deg); (b) Bias angle (control input), β (deg); (c) yaw rate, r (deg/s); (d) lateral velocity, v (m/s); (e) lateral force, F_y (N); and (f) side moment, M_y (Nm).

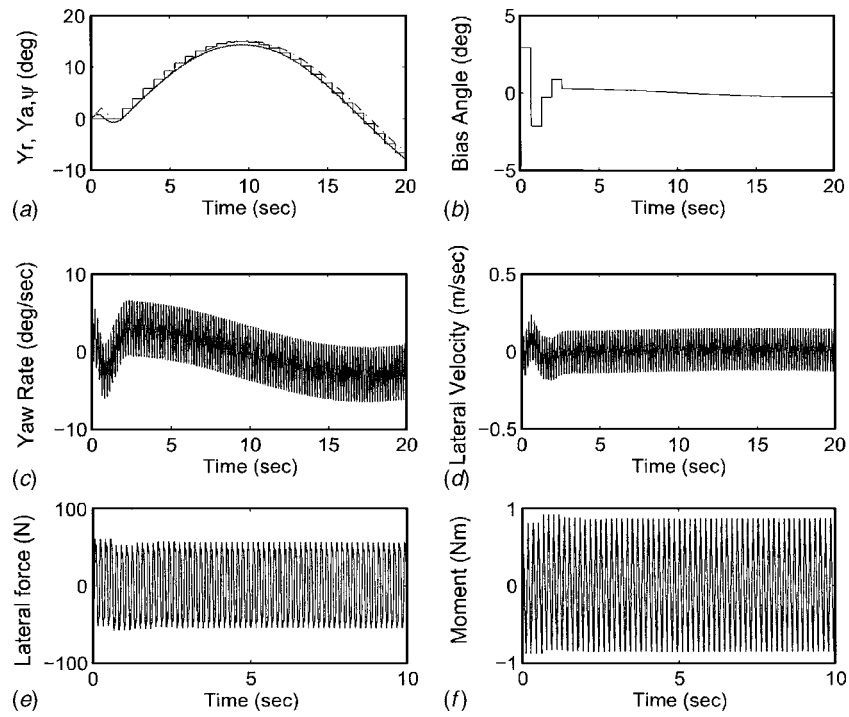


Fig. 12 Inverse control: Frequency of flapping=6 Hz, $d_{cgf}=0$ m for $\psi^* = 15$ deg: (a) reference heading angle, Y_r (staircase); modified heading angle, Y_a (broken line); and actual heading angle, ψ (solid line) (deg). (b) Bias angle (control input), β (deg); (c) yaw rate, r (deg/s); (d) lateral velocity, v (m/s); (e) lateral force, F_y (N); and (f) side moment, M_y (Nm).

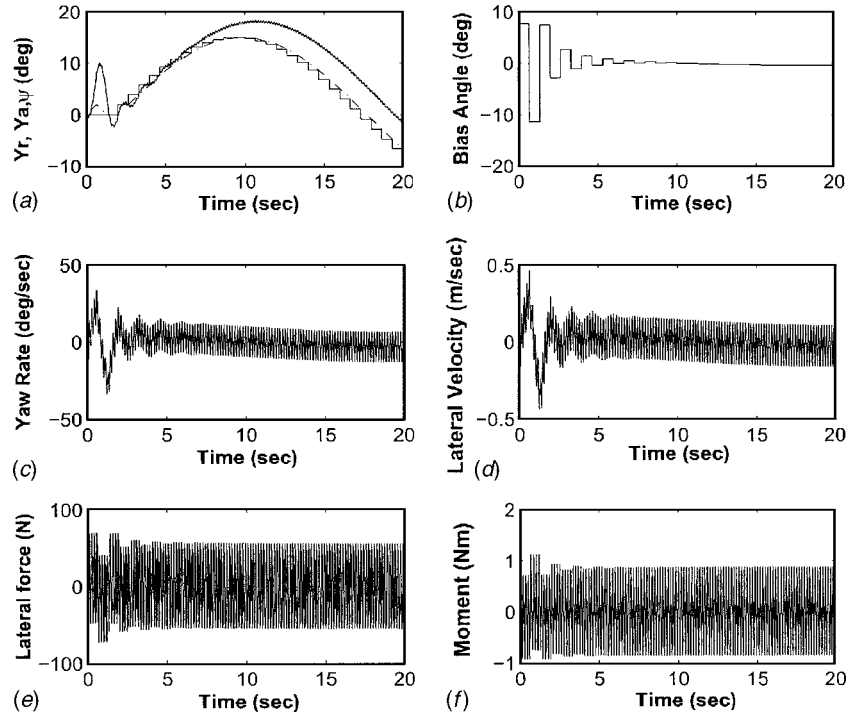


Fig. 13 Inverse control: Frequency of flapping=6 Hz, $d_{cgf}=0.15$ m for $\psi^* = 15$ deg: (a) reference heading angle, Y_r (staircase); modified heading angle, Y_a (broken line); and actual heading angle, ψ (solid line) (deg). (b) Bias angle (control input), β (deg); and (c) yaw rate, r (deg/s); (d) lateral velocity, v (m/s); (e) lateral force, F_y (N); and (f) side moment, M_y (Nm).

=0.15 m are relatively less stable compared to the zero dynamics for $d_{cgf}=0$. Note that $G_a(z)$ has a zero at 0.0965 for $d_{cgf}=0$ and at a lesser stable location -0.75 for $d_{cgf}=0.15$ m.

Case 4. Inverse control: Frequency of Oscillation 6 Hz, $d_{cgf}=0$ and $d_{cgf}=0.15$ (m). The first simulation performed here is for $d_{cgf}=0$ and frequency 6 Hz. The results are shown in Fig. 12. Yaw angle tracking is achieved although intersample oscillations of comparatively large magnitude are observed. The bias angle (control input) required is <3 deg.

Simulation for $d_{cgf}=0.15$ m has also been performed, and results are shown in Fig. 13. In the closed-loop system, approximate yaw angle tracking is accomplished, but larger intersample oscillations appear. Again it is found that the inverse controller designed for $d_{cgf}=0$ performs better compared to the controller designed for $d_{cgf}=0.15$ m precisely due to the reasons indicated in case 3 for the frequency of oscillation 8 Hz.

7 Conclusion

In this paper, optimal as well as inverse yaw-plane control of a biorobotic AUV using pectoral-like fins was considered. For maneuvering the BAUV, the bias angle was treated as control input. CFD and Fourier series expansion were used to parameterize the effect of this control input on the hydrodynamical force and moment produced by the flapping foil. For the purpose of design, a discrete-time model was obtained and a minimum phase representation was derived for controller design. Then an optimum control law for the regulation of the yaw angle to set points and an inverse control law for the trajectory control of the modified output were derived. The bias angle of the flapping foils was updated at discrete intervals (multiple of the fundamental period). In the closed-loop system, the modified output and the actual yaw trajectory were found to be sufficiently close to the desirable heading angle commands. From these results, one concludes that accurate yaw angle control along time-varying paths can be accomplished using oscillating fins with relatively small (<3 deg) overall changes in the bias angle. Furthermore, improved performance of the control system can be obtained when the frequency of oscillation of the fins increases.

This paper provides an interdisciplinary approach, which combines the CFD analysis and control theory, for the design of control systems for BAUVs. But there are several questions remain to be answered in this area. Certainly, the treatment of nonlinearities; sensor and actuator dynamics; noise, wave forces, and parameter uncertainties; etc., is important. The effect of vortices shed by the body on the fins is yet another interesting problem for future research.

References

- [1] Azuma, A., 1992, *The Bio-Kinetics of Flying and Swimming*, Springer-Verlag, Berlin.
- [2] Sfakiotakis, M., Lane, D. M., and Davies, J. B. C., 1999, "Review of Fish Swimming Modes for Aquatic Locomotion," *IEEE J. Ocean. Eng.*, **24**(2), pp. 237–253.
- [3] Triantafyllou, G. S., and Triantafyllou, M. S., 1995, "An Efficient Swimming Machine," *Sci. Am.*, **272**, pp. 64–70.
- [4] Bandyopadhyay, P. R., Castano, J. M., Rice, J. Q., Philips, R. B., Nedderman, W. H., and Macy, W. K., 1997, "Low-Speed Maneuvering Hydrodynamics of Fish and Small Underwater Vehicles," *ASME J. Fluids Eng.*, **119**, pp. 136–144.
- [5] Lauder, G. V., and Drucker, E. G., 2004, "Morphology and Experimental Hydrodynamics of Fish Fin Control Surfaces," *IEEE J. Ocean. Eng.*, **29**, pp. 556–571.
- [6] Walker, J. A., 2004, "Kinematics and Performance of Maneuvering Control Surfaces in Teleost Fishes," *IEEE J. Ocean. Eng.*, **29**, pp. 572–584.
- [7] Triantafyllou, M. S., Techet, A. H., and Hover, F. S., 2004, "Review of Experimental Work in Biomimetic Foils," *IEEE J. Ocean. Eng.*, **29**, pp. 585–594.
- [8] Mittal, R., 2004, "Computational Modeling in Biohydrodynamics: Trends,

- Challenges, and Recent Advances," *IEEE J. Ocean. Eng.*, **29**, pp. 595–604.
- [9] Westneat, M. W., Thorsen, D. H., Walker, J. A., and Hale, M. E., 2004, "Structure, Function, and Neural Control of Pectoral Fins in Fishes," *IEEE J. Ocean. Eng.*, **29**, pp. 674–683.
- [10] Bandyopadhyay, P. R., Castano, J. M., and Dick, J., 1999, "Biologically-Inspired Bodies Under Surface Waves—Part 1: Load Measurement," *ASME J. Fluids Eng.*, **121**, pp. 469–478.
- [11] Bandyopadhyay, P. R., Singh, S. N., and Chockalingam, F., 1999, "Biologically-Inspired Bodies Under Surface Waves—Part 2: Theoretical Control of Maneuvering," *ASME J. Fluids Eng.*, **121**, pp. 479–487.
- [12] Bandyopadhyay, P. R., 2002, "Maneuvering Hydrodynamics of Fish and Small Underwater Vehicles," *Integr. Comp. Biol.*, **42**, pp. 102–117.
- [13] Triantafyllou, M. S., Techet, A., and Hover, F., 2003, "Review of Experimental Work in Biomimetic Foils," 13th International Symposium on Unmanned Untethered Submersible Technology (UUST), New England Center, Durham, NH.
- [14] Martin, C. B., Hover, F. S., and Triantafyllou, M. S., 2001, "Maneuvering Performance of a Rolling and Pitching Wing," 12th International Symposium on Unmanned Untethered Submersible Technology," New England Center, Durham, NH.
- [15] Yamamoto, I., Terada, Y., Nagamatu, T., and Imaizumi, Y., 1995, "Propulsion System With Flexible/Rigid Oscillating Fin," *IEEE J. Ocean. Eng.*, **20**(1), pp. 23–30.
- [16] Kato, N., 2002, "Pectoral Fin Controllers," *Neurotechnology for Biometric Robots*, MIT Press, Cambridge, MA, pp. 325–350.
- [17] Kato, N., 2000, "Performance in the Horizontal Plane of a Fish Robot With Mechanical Pectoral Fins," *IEEE J. Ocean. Eng.*, **25**(1), pp. 121–129.
- [18] Mittal, R., Utturkar, Y., and Udaykumar, H. S., 2002, "Computational Modeling and Analysis of Biomimetic Flight Mechanisms," AIAA Paper No. 2002–0865.
- [19] Udaykumar, H. S., Mittal, R., Rampunggoon, P., and Khanna, A., 2001, "A Sharp Interface Cartesian Grid Method for Simulating Flows With Complex Moving Boundaries," *J. Comput. Phys.*, **174**, 345–380.
- [20] Ye, T., Mittal, R., Udaykumar, H. S., and Shyy, W., 1999, "An Accurate Cartesian Grid Method for Simulation of Viscous Incompressible Flows With Complex Immersed Boundaries," *J. Comput. Phys.*, **156**, 209–240.
- [21] Ramamurti, R., Lohner, R., and Sandberg, W., 1996, "Computation of the Unsteady-Flow Past a Tuna With Caudal Fin Oscillation," *Adv. Fluid Mech. Series*, **9**, pp. 169–178.
- [22] Najjar, F. M., Mittal, R., Rampunggoon, P., and Khanna, A., 2003, "Simulations of Complex Flows and Fluid-Structure Interaction Problems on Fixed Cartesian Grids," ASME Paper No. FEDSM2003–45577.
- [23] Lee, J. S., Kim, C., and Rho, O. H., 2003, "The Modification of Airfoil Shape for Optimal Aerodynamic Performance on Flapping-Airfoil in Low-Reynolds Number Flow," AIAA Paper No. 2003–421.
- [24] Mittal, R., 2004, "Computational Modeling in Bio-Hydrodynamics: Trends, Challenges and Recent Advances," *IEEE J. Ocean. Eng.*, **29**(3), pp. 595–604.
- [25] Koochesfahani, M. M., 1987, "Vertical Patterns in the Wake of an Oscillating Airfoil," AIAA 25th Aerospace Sciences Meeting, Reno, AIAA Paper No. 87–0111.
- [26] Mittal, R., Akhtar, I., Bozkurtas, M., and Najjar, F. M., 2003, "Towards a Conceptual Model of a Bio-Robotic AUV: Pectoral Fin Hydrodynamics," 13th International Symposium on Unmanned Untethered Submersible Technology, Durham, NH, August.
- [27] Meneveau, C., Lund, T. S., and Cabot, W. H., 1996, "A Lagrangian Dynamic Subgrid-Scale Model of Turbulence," *J. Fluid Mech.*, **319**, pp. 353–385.
- [28] Bozkurtas, M., Dong, H., Mittal, R., and Najjar, F., 2005, "Towards Numerical Simulation of Flapping Foils on Fixed Cartesian Grids," Reno, NV, January, AIAA Paper No. 2005–0079.
- [29] Dong, H., Mittal, R., Bozkurtas, M., and Najjar, F., 2005, "Wake Structure and Performance of Finite Aspect-Ratio Flapping Foils," Reno, NV, January, AIAA Paper No. 2005–0081.
- [30] Soria, J., and Cantwell, B. J., 1993, "Identification and Classification of Topological Structures in Free Shear Flows," *Eddy Structure Identification in Free Turbulent Shear Flows*, J. P. Bonnet and M. N. Glauser, eds., pp. 379–390.
- [31] Fossen, T. I., 1999, *Guidance and Control of Ocean Vehicles*, Wiley, New York.
- [32] Singh, S. N., Simha, A., and Mittal, R., 2004, "Biorobotic AUV Maneuvering by Pectoral Fins: Inverse Control Design Based on CFD Parameterization," *IEEE J. Ocean. Eng.*, **29**(3), pp. 777–785.
- [33] Ridley, P., Fontan, J., and Corke, P., 2003, "Submarine Dynamic Modeling," *Australian Conference on Robotics and Automation*, Brisbane, Australia, December.
- [34] Davison, E. J., 1976, "The Robust Control of a Servomechanism Problem for Linear Time-Invariant Multivariable Systems," *IEEE Trans. Autom. Control*, **21**, pp. 25–34.
- [35] Phillips, C. L., and Nagle, H. T., 1995, "Digital Control System Analysis and Design," Prentice-Hall, Englewood Cliffs, NJ.
- [36] Chen, C. T., 1998, *Linear System Theory and Design*, Oxford University Press, London.